ChemComm

COMMUNICATION

Cite this: *Chem. Commun.*, 2018, **54**, 5090

Received 8th March 2018,
Accepted 11th April 2018

DOI: 10.1039/c8cc01889h

rsc.li/chemcomm

Ultra-long-term cycling stability of an integrated carbon–sulfur membrane with dual shuttle-inhibiting layers of graphene "nets" and a porous carbon skin†

Mingkai Liu,‡[a] Qinghua Meng,‡[a] Zhiyuan Yang,[a] Xinsheng Zhao*[b] and Tianxi Liu *[ac]

An integrated carbon–sulfur (CSG/PC) membrane with dual shuttle-inhibiting layers was prepared by inserting graphene "nets" and a porous carbon (PC) skin, and the membrane achieved an extraordinary cycling stability up to 1000 cycles with an average Coulombic efficiency of ~100%.

Lithium–sulfur (Li–S) batteries, based on the multielectron-transfer reactions occurring between sulphur and lithium, *i.e.*, $S_8 + 16Li^+ + 16e^- \rightarrow 8Li_2S$, with an ultra-high theoretical energy density of 2600 W h kg^{-1} and an extremely high theoretical capacity of 1672 mA h g^{-1} have been considered as one of the most promising energy-storage systems.[1] Meanwhile, the energy density achieved by Li–S batteries is 3 to 5 times higher than that achieved by the state-of-the-art lithium ion batteries; also, Li–S batteries have unique characteristics such as low cost, lightweightedness and nontoxicity.[2] However, the practical use of Li–S batteries has been limited as a result of low utilization and poor cycling life of active sulfur cathode.[3] These disadvantages are mainly due to the dissolution and shuttling effect of polysulfide intermediates (Li_2S_n, $4 \leq n \leq 8$) in the organic electrolyte.[4] However, the electronic insulation of sulfur and its insoluble discharge products (Li_2S/Li_2S_2) can further cause sluggish reaction kinetics for the sulfur cathodes.[5]

Many approaches have been carried out to overcome these drawbacks, and they mainly focus on two basic strategies: (i) inside and (ii) outside aspects.[6] On the one hand, a number of methods have been utilized to confine active sulfur elements inside the cathode. Numerous porous materials, especially carbon matrices with mesoporous structures, have been developed to act as physical barriers to prevent Li_2S_n from being dissolved into an organic electrolyte.[1b,4a,7] In addition, mesoporous matrices can efficiently enhance sulfur loading levels. On the other hand, an effective interlayer, mainly consisting of carbon nanotubes, carbon nanofibers and conductive polymers, can be inserted between the separator and sulfur cathode to mitigate the shuttling effect of Li_2S_n.[8] Improved electrochemical performances have been achieved for Li–S batteries according to these two strategies.[7,9]

However, the diffusion and shuttling of Li_2S_n cannot be completely prevented by utilizing mesoporous materials alone.[10] Meanwhile, the hindering effect of interlayers with micropores is also limited. Free-standing interlayers with large thickness may also hinder the efficient transport of ions and electrons. Therefore, development of high-performance carbon–sulfur cathodes with hierarchical architectures that simultaneously enhance the electrical conductivity of carbon–sulfur cathodes and inhibit the shuttling of Li_2S_n still remains a great challenge.

In this study, an integrated carbon–sulfur membrane consisting of carbon–sulfur (CS) nanoparticles with dual "shuttle-inhibiting" layers of graphene "nets" (CSG) and a closely attached porous carbon (PC) skin, referred to as CSG/PC membrane, has been developed. Porous carbon nanoparticles (Fig. S1, ESI†) with an ultra-high specific surface area up to 1380 $m^2\ g^{-1}$ (Fig. S2, ESI†) are used as a template for enhancing the loading of active sulfur. The inserted graphene sheets can effectively improve the electrical conductivity of the obtained CSG/PC membrane while acting as "trapping nets" to restrict the "shuttling" of polysulfide intermediates. Also, a porous carbon (PC) skin, consisting of graphene sheets and carbon nanoparticles with a specific surface area of 663 $m^2\ g^{-1}$ (Fig. S3, ESI†), is closely attached to the bottom of the CSG film. This PC skin with a thickness of ~2 μm can effectively inhibit the "shuttling" of polysulfide intermediates while providing sufficient channels for the rapid transport of electrons and lithium ions (Li^+) simultaneously. As a result, this CSG/PC membrane shows greatly improved electrochemical performances including a high specific capacity of 1221 mA h g^{-1},

[a] *School of Chemistry and Chemical Engineering, Jiangsu Key Laboratory of Green Synthetic Chemistry for Functional Materials, Jiangsu Normal University, Xuzhou 221116, China. E-mail: txliu@dhu.edu.cn*
[b] *School of Physics and Electronic Engineering, Jiangsu Normal University, Xuzhou 221116, China. E-mail: Xinshengzhao@jsnu.edu.cn*
[c] *State Key Laboratory for Modification of Chemical Fibers and Polymer Materials, College of Materials Science and Engineering, Donghua University, Shanghai 201620, China*

† Electronic supplementary information (ESI) available: SEM, TGA results and Experimental section. See DOI: 10.1039/c8cc01889h

‡ These authors contributed equally to this work.

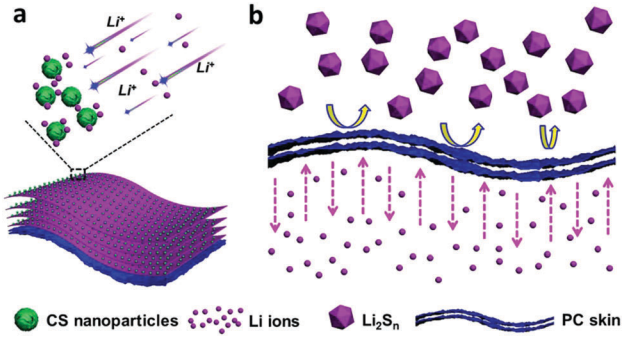

Fig. 1 Schematic representation of (a) rapid attraction of Li^+ by carbon–sulfur (CS) nanoparticles and (b) "shuttling" inhibitory effect of Li_2S_n caused by the closely attached porous carbon (PC) skin.

good rate capability and ultra-long-term cycling stability (1000 cycles with a capacity retention of 88.9%) with a high Coulombic efficiency of ~100%. This multi-layer CSG/PC membrane with dual capacity protection architectures can provide new strategies for developing high-performance electrode materials in energy storage fields.

Fig. 1a schematically shows that the inserted CS nanoparticles can attract a large amount of Li^+ *via* interfacial reactions. Graphene sheets used for uniform dispersion of CS nanoparticles can greatly improve the electrical conductivity of the prepared CSG film while acting as "trapping nets" to physically restrict the shuttling effect of polysulfides. Herein, a PC skin consisting of graphene sheets and porous carbon nanoparticles is closely attached to the bottom of CSG film. The attached PC skin can provide sufficient transport channels for electrons and Li^+ while playing an important role as the second defensive layer for restricting the "shuttling" of polysulfide intermediates (Fig. 1b).

The SEM image of the CSG/PC film with a thickness of ~100 μm is provided in Fig. 2a. High-resolution SEM images of the cross-section of this CSG/PC film (Fig. 2b and c) confirm that CS nanoparticles can be uniformly dispersed using graphene sheets without any aggregations. SEM images of the CSG film at low and high magnifications are also provided (Fig. S4, ESI†). The layered structures and high CS content in the CSG/PC membrane can also be confirmed in this study. The EDS mappings of the selected area in the cross-section (Fig. 2d) apparently confirm the presence of carbon (C) and sulfur (S) elements (Fig. 2e and f, respectively), indicating that active S is uniformly distributed throughout the membrane of the CSG/PC film. The hardly detected O element mapping (Fig. 2g) can be due to the efficient chemical reduction effect of hydrazine vapour. Furthermore, energy spectrum of the selected area is shown in Fig. 2h. Apparent characteristic peaks of S are obtained, and a high S content of 90.1 wt% is successfully achieved. Meanwhile, the good flexibility of this CSG/PC membrane ensures that it can be directly used as a binder-free cathode (Fig. S5, ESI†).

Fig. 3a exhibits the XRD patterns of pure S, the CSG/PC film and the pure carbon–graphene (CG) hybrid. The XRD pattern of the CG hybrid exhibits a broad peak at around 25°, indicating the efficient reduction of GO due to the complete removal of oxygen-containing groups by hydrazine vapour. The CSG/PC film shows similar XRD diffraction peaks to those of pure S materials as a result of the effective loading of active sulfur by the carbon nanoparticles. The TGA curves of pure S, the CSG/PC film and the CG hybrid (Fig. 3b) indicate that the weight percentage of active sulfur in the CSG/PC film is as high as 90.1%. The XPS survey spectra of the CSG/PC film (Fig. 3c) proves the existence of S 2s and S 2p peaks, indicating the successful incorporation of active sulfur into the prepared CSG film. The XPS spectra of S 2p at around 165 eV can be divided into two individual peaks, S $2p_{1/2}$ and S $2p_{3/2}$. Herein, the S $2p_{1/2}$ and S $2p_{3/2}$ peaks at 165.5 eV and 164.1 eV (Fig. 3d), respectively, with an intensity ratio of about 1 : 2 can be ascribed to the characteristic solid sulfur in the CSG/PC membrane.[4b,11] Also, the nearly diminished peaks corresponding to C–O and C═O groups in the C 1s spectra (Fig. 3e) indicate that the conjugated

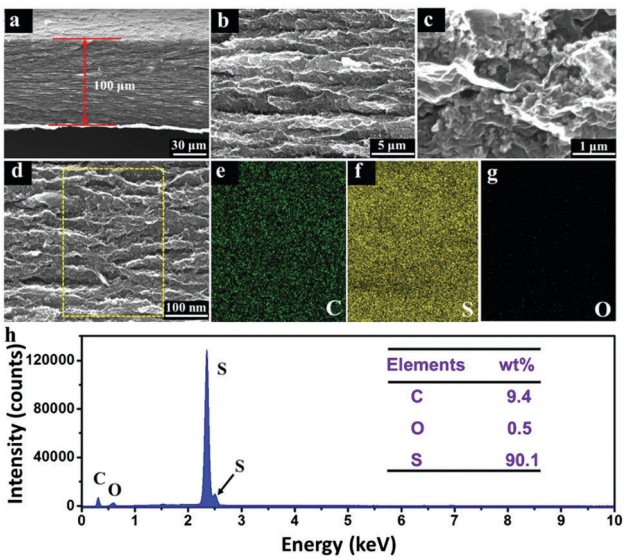

Fig. 2 (a–c) SEM images of the CSG film at different magnifications; (d) SEM image of the selected area of the CSG film and the corresponding mapping images of (e) C, (f) S and (g) O elements; and (h) energy spectra of the CSG film along with the weight percentages of C, O and S elements.

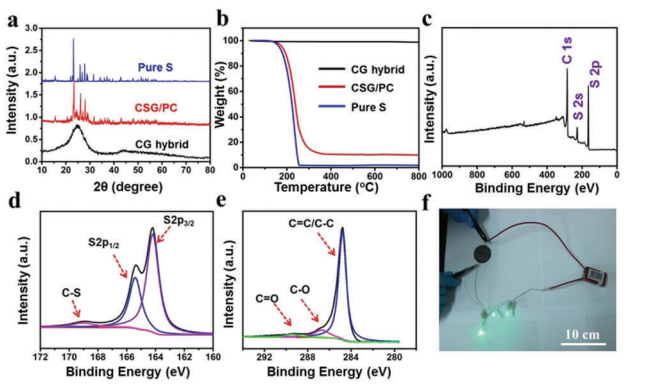

Fig. 3 (a) XRD patterns and (b) TGA curves of pure S, the CSG film and the pure CG hybrid; XPS analysis of the CSG film for the (c) survey spectrum, (d) S 2p spectrum and (e) C 1s spectrum; and (f) a stable circuit with the CSG film replacing the copper wire.

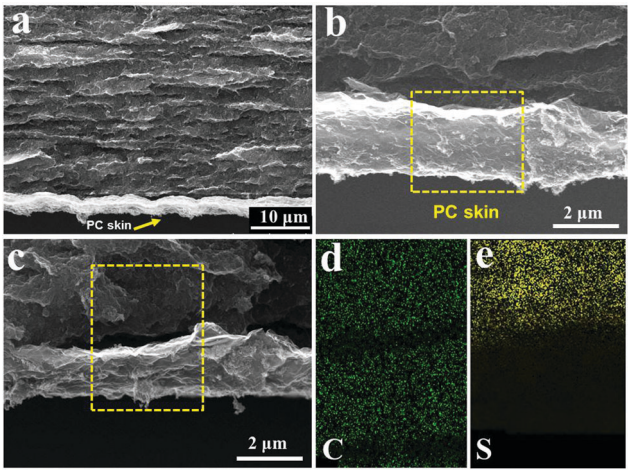

Fig. 4 SEM images of (a) the CSG/PC membrane and (b and c) the PC skin at low and high magnifications. (d and e) Corresponding EDS mappings of C and S elements.

structures of graphene sheets have been recovered. The obtained CSG/PC film with an electrical conductivity of 79 S cm^{-1} can be used as a substitute for copper wire in a closed circuit (Fig. 3f).

Fig. 4a exhibits the SEM image of the cross-section of the CSG/PC membrane. An ultra-thin PC skin with a thickness of ~2 μm can be clearly observed at the bottom of the CSG film. The SEM image at high magnification (Fig. 4b) indicates that the PC skin is closely attached to the bottom of the CSG film. EDS mappings are used to detect the distribution of active S in the CSG and PC interface, as shown in Fig. 4c–e. It can be seen that C is distributed throughout the selected area of the CSG/PC membrane, whereas S can only be detected in the CSG region. These features of the CSG/PC membrane confirm that a PC skin with a porous structure acting as the second "shuttling" inhibition layer has been constructed at the bottom of the CSG film.

Electrochemical measurements have been carried out to verify the positive effect of the PC skin on the CSG film. Fig. 5a exhibits the cyclic voltammograms (CVs) of the CSG/PC membrane cathode at a scan rate of 0.1 mV s^{-1} for the initial three cycles. The two cathodic peaks at about 2.32 and 2.03 V (*vs.* Li/Li^+) can be due to the transformation of S_8 molecules to long-chain soluble lithium polysulfides (Li_2S_n, $4 \leq n \leq 8$), followed by the formation of short-chain insoluble discharge products (Li_2S_2 / Li_2S).[12] Also, the subsequent anodic peaks at 2.30 and 2.42 V (*vs.* Li/Li^+) can be assigned to the oxidation of Li_2S_2/Li_2S to Li_2S_8.[13] The CV curve at the 3rd cycle almost completely overlaps the one at the 2nd cycle, implying that the CSG/PC membrane has good electrochemical stability in highly reversible redox reactions. Fig. 5b shows the galvanostatic discharge/charge voltage profiles of the CSG/PC membrane cathode for the first three cycles at 0.1C (1C = 1672 mA g^{-1}). Two potential plateaus at about 2.33 and 2.04 V (*vs.* Li/Li^+) can be clearly observed during the discharge process, which are consistent with those observed for the typical two-step reactions of S_8 molecules to form Li_2S_2/Li_2S, as demonstrated in the CV curves. Herein, a Li–S battery with the CSG/PC membrane cathode exhibits a reversible specific capacity of 1221 mA h g^{-1}, which is comparable with the result (1205 mA h g^{-1}) of the CSG film cathode.

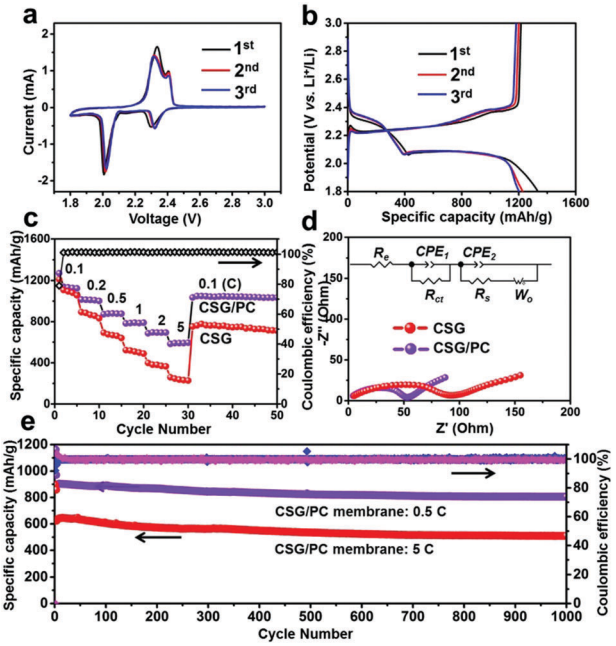

Fig. 5 Electrochemical performances of Li–S batteries based on CSG films and CSG/PC membrane cathodes. (a) CV curves at 0.1 mV s^{-1} and (b) discharge/charge curves at 0.1C of Li–S batteries with CSG/PC membrane cathodes. (c) Rate capabilities and (d) Nyquist plots of Li–S batteries based on CSG films and CSG/PC membrane cathodes. (e) Long-term cycling performances of CSG/PC membrane cathodes at 0.5 and 5C along with their Coulombic efficiencies.

Rate capabilities of CSG/PC membranes and CSG film cathodes at different current rates are presented in Fig. 5c. The Li–S battery with CSG/PC membrane cathode delivers larger discharge capacities of 1218, 1003, 882, 775, 690 and 588 mA h g^{-1} at 0.1, 0.2, 0.5, 1, 2 and 5C, respectively, indicating that this CSG/PC membrane can effectively utilize active sulfur even at high current densities up to 5C. However, the discharge capacities of the CSG films sharply decrease with an increase in the current density. A specific capacity of 215 mA h g^{-1} for the CSG film cathode is obtained at 5C, which is much lower than the result (590 mA h g^{-1}) for the CSG/PC membrane cathode. Meanwhile, the discharge capacity of the CSG/PC membrane cathode can be recovered to 1045 mA h g^{-1} when the current density is decreased to 0.1C, and an average Coulombic efficiency of ~100% is also observed, which indicates that the structure of the CSG/PC membrane is very stable even after it is subjected to high current densities.[14]

Moreover, electrochemical impedance spectroscopy (EIS) was conducted to ascertain the interfacial behavior of CSG/PC membranes and CSG film cathodes. After being cycled for 10 times at 1C, EIS tests of Li–S batteries based on CSG/PC and CSG cathodes were carried out using a combined system of Solartron and Princeton (Fig. 5d). The intersection of the *X*-axis and the semicircle of the CSG/PC membrane, which can be ascribed to the Ohmic resistance (R_e) between the electrode and the electrolyte,[15] was as low as 3.9 Ω. The diameter of its semicircle (47.7 Ω), which is associated with the charge transfer resistance (R_{ct}),[2a,16] was much lower than that of the CSG cathode (85.5 Ω). These greatly improved interfacial reaction kinetics can be attributed to the

diminished shuttling effect of polysulfide intermediates and the enhanced reutilization of dissolved polysulfide intermediates.[3c,17] According to the equivalent circuit (inset in Fig. 5d), impedance parameters were calculated based on the two Nyquist plots of CSG/PC membranes and CSG films, and these parameters are listed in Table S1 (ESI†). Herein, the effectively reduced interfacial impedances of CSG/PC membranes could be ascribed to the efficient assistance of the PC skin attached to the bottom of CSG films.

Long-term cycling performances of the CSG/PC membrane cathodes have been tested at current densities of 0.5 and 5C (Fig. 5e). The capacity of the CSG/PC membrane cathode is stabilized around 800 mA h g^{-1} after 1000 cycles (0.5C), corresponding to a capacity retention of 88.9% and a much small capacity fading of only 0.011% per cycle. Furthermore, this CSG/PC membrane cathode also exhibits excellent cycling stability even at a high current density of 5C with a high specific capacity of 505 mA h g^{-1} maintained after 1000 cycles. Meanwhile, the average Coulombic efficiency of the CSG/PC membrane cathode is surprisingly close to 100% during the whole cycling process. Comparatively, the CSG film exhibits a serious capacity fading during the long-term cycling process with a capacity of 255 mA h g^{-1} maintained after 1000 cycles, which is much lower than its initial specific capacity of 755 mA h g^{-1} at 0.5C (Fig. S6, ESI†). Compared to the poor cycle life of the CSG film, the outstanding cycling performance of the CSG/PC membrane can be ascribed to the effective dual protections from the inserted graphene ''nets'' and the attached PC skin. The hardly increased impedance parameters of the CSG/PC membrane obtained for the 1000th cycle compared with the results obtained for the 10th cycle further confirm its good cycling stability (Fig. S7 and Table S2, ESI†).

In summary, an integrated CSG/PC membrane with a high sulfur content of 90.1% has been developed with an ultra-thin PC skin attached to the bottom of the CSG film. Porous carbon nanoparticles acting as deposition matrices ensure a high sulfur loading of 90.1%, which further results in huge porous structures inside the obtained CSG/PC membrane. The inserted graphene sheets play an important role in enhancing the electrical conductivity and accelerating the rapid transport of electrons. The ''shuttling effect'' of the polysulfide intermediates is doubly restricted by the inserted graphene ''nets'' and the closely attached PC skin. As a result, Li–S batteries with CSG/PC membrane cathodes exhibit excellent electrochemical performances including a high specific capacity of 1221 mA h g^{-1} and an excellent rate capability. Especially, the dual protections from the graphene ''nets'' and the PC skin endow CSG/PC membranes with an extraordinary cycling stability up to 1000 cycles and Coulombic efficiencies close to 100%. Moreover, the dual protection approach presented herein can offer a facile and efficient strategy for fabricating high-performance sulfur cathodes for Li–S batteries with ultra-long life.

This study was supported by the National Natural Science Foundation of China (No. 51373037, 51433001 and 51703087), PAPD, and Natural Science Foundation of Jiangsu Province (BK20150238).

Conflicts of interest

There are no conflicts to declare.

Notes and references

1 (*a*) Y. S. Su, Y. Fu, T. Cochell and A. Manthiram, *Nat. Commun.*, 2013, **4**, 2985; (*b*) H. Wang, W. Zhang, H. Liu and Z. Guo, *Angew. Chem., Int. Ed.*, 2016, **55**, 3992; (*c*) T.-Z. Hou, W.-T. Xu, X. Chen, H.-J. Peng, J.-Q. Huang and Q. Zhang, *Angew. Chem., Int. Ed.*, 2017, **56**, 8178; (*d*) J. Wang, K. Xie and B. Wei, *Nano Energy*, 2015, **15**, 413.
2 (*a*) N. Liu, B. Huang, W. Wang, H. Shao, C. Li, H. Zhang, A. Wang, K. Yuan and Y. Huang, *ACS Appl. Mater. Interfaces*, 2016, **8**, 16101; (*b*) R. Fang, S. Zhao, Z. Sun, D. W. Wang, H. M. Cheng and F. Li, *Adv. Mater.*, 2017, 1606823.
3 (*a*) Y. Cui and Y. Fu, *ACS Appl. Mater. Interfaces*, 2015, **7**, 20369; (*b*) H. J. Peng, D. W. Wang, J. Q. Huang, X. B. Cheng, Z. Yuan, F. Wei and Q. Zhang, *Adv. Sci.*, 2016, **3**, 1500268; (*c*) H. Yao, K. Yan, W. Li, G. Zheng, D. Kong, Z. W. Seh, V. K. Narasimhan, Z. Liang and Y. Cui, *Energy Environ. Sci.*, 2014, **7**, 3381.
4 (*a*) X. Fang, W. Weng, J. Ren and H. Peng, *Adv. Mater.*, 2016, **28**, 491; (*b*) X. Liu, J. Q. Huang, Q. Zhang and L. Mai, *Adv. Mater.*, 2017, **29**, 1601759; (*c*) S. H. Yu, B. Lee, S. Choi, S. Park, B. H. Hong and Y. E. Sung, *Chem. Commun.*, 2016, **52**, 3203; (*d*) A. Shyamsunder, W. Beichel, P. Klose, Q. Pang, H. Scherer, A. Hoffmann, G. K. Murphy, I. Krossing and L. F. Nazar, *Angew. Chem., Int. Ed.*, 2017, **56**, 6192.
5 J. Liu, L. Yuan, K. Yuan, Z. Li, Z. Hao, J. Xiang and Y. Huang, *Nanoscale*, 2016, **8**, 13638.
6 H. Wang, C. Zhang, Z. Chen, H. K. Liu and Z. Guo, *Carbon*, 2015, **81**, 782.
7 (*a*) X. Fang and H. Peng, *Small*, 2015, **11**, 1488; (*b*) J. Wang, Z. Zhang, X. Zhang, X. Yin, X. Li, X. Liu, F. Kang and B. Wei, *Nano Energy*, 2017, **39**, 647; (*c*) S. Jiang, B. Zhao, R. Ran, R. Cai, M. O. Tade and Z. Shao, *RSC Adv.*, 2014, **4**, 9367.
8 (*a*) L. Chai, J. Wang, H. Wang, L. Zhang, W. Yu and L. Mai, *Nano Energy*, 2015, **17**, 224; (*b*) C. L. Lee and I. D. Kim, *Nanoscale*, 2015, **7**, 10362; (*c*) J. Huang, Q. Zhang and F. Wei, *Energy Storage Materials*, 2015, **1**, 127.
9 (*a*) J. Zhu, D. Yang, Z. Yin, Q. Yan and H. Zhang, *Small*, 2014, **10**, 3480; (*b*) T. Z. Zhuang, J. Q. Huang, H. J. Peng, L. Y. He, X. B. Cheng, C. M. Chen and Q. Zhang, *Small*, 2016, **12**, 381; (*c*) J. Balach, T. Jaumann, M. Klose, S. Oswald, J. Eckert and L. Giebeler, *Adv. Funct. Mater.*, 2015, **25**, 5285; (*d*) H.-S. Kang and Y.-K. Sun, *Adv. Funct. Mater.*, 2016, **26**, 1225.
10 Y. Yang, G. Yu, J. J. Cha, H. Wu, M. Vosgueritchian, Y. Yao, Z. Bao and Y. Cui, *ACS Nano*, 2011, **5**, 9187.
11 S. Rehman, T. Tang, Z. Ali, X. Huang and Y. Hou, *Small*, 2017, **13**, 1700087.
12 J. Zhu, Y. Ge, D. Kim, Y. Lu, C. Chen, M. Jiang and X. Zhang, *Nano Energy*, 2016, **20**, 176.
13 (*a*) J. L. Shi, C. Tang, H. J. Peng, L. Zhu, X. B. Cheng, J. Q. Huang, W. Zhu and Q. Zhang, *Small*, 2015, **11**, 5243; (*b*) J. Song, Z. Yu, M. L. Gordin and D. Wang, *Nano Lett.*, 2016, **16**, 864.
14 (*a*) R. Fang, S. Zhao, P. Hou, M. Cheng, S. Wang, H. M. Cheng, C. Liu and F. Li, *Adv. Mater.*, 2016, **28**, 3374; (*b*) Y. Liu, G. Li, J. Fu, Z. Chen and X. Peng, *Angew. Chem., Int. Ed.*, 2017, **56**, 6176.
15 (*a*) L. Ni, Z. Wu, G. Zhao, C. Sun, C. Zhou, X. Gong and G. Diao, *Small*, 2017, **13**, 1603466; (*b*) L. Sun, W. Kong, M. Li, H. Wu, K. Jiang, Q. Li, Y. Zhang, J. Wang and S. Fan, *Nanotechnology*, 2016, **27**, 075401.
16 X. B. Cheng, H. J. Peng, J. Q. Huang, F. Wei and Q. Zhang, *Small*, 2014, **10**, 4257.
17 C. H. Chang, S. H. Chung and A. Manthiram, *Small*, 2016, **12**, 174.